ELSEVIER

Journal of Structural Geology 29 (2007) 802–818

JOURNAL OF STRUCTURAL GEOLOGY

www.elsevier.com/locate/jsg

Disentangling tectonic cycles along a multiply deformed terrane margin: Structural and metamorphic evidence for mid-crustal reworking of the Angul granulite complex, Eastern Ghats Belt, India

Meenakshi Sarkar, Saibal Gupta*, M.K. Panigrahi

Department of Geology and Geophysics, Indian Institute of Technology, Kharagpur 721 302, India

Received 20 May 2006; received in revised form 5 January 2007; accepted 17 January 2007
Available online 7 February 2007

Abstract

Modern orogenic belts may be rifted and reworked during later tectonic cycles. In ancient collision zones, such as the Eastern Ghats Belt (EGB), India, identification of such processes is complicated by the multiply folded nature of the exposed deep crustal section. Along the northern EGB margin, (M1) granulite facies metamorphism (~7–8 kbar, >760 °C) at ~960–930 Ma outlasted D_1 fabric formation, and D_2 isoclinal folding and shearing. N-S trending mafic dykes and N-S trending, west-dipping shear zones accompanied D_3 extension. Syn-D_3 cooling and decompression caused garnet breakdown in mafic granulites. Granite and pegmatite emplacement at c. 850 Ma accompanied uplift on E-W trending, subvertical D_4 shear planes. Top-to-the-south thrusting on WNW-ESE trending, north-dipping D_5 shears resulted in regional-scale fabric reorientation. During M2 amphibolite facies metamorphism (~5.5 kbar, 630 °C) at c. 700 Ma following D_5, garnet reformed in mafic granulites, and stabilized within syn-D_3 mafic dykes and syn-D_4 granites. Thus, the terrane margin experienced heating, loading and uplift during a first tectonic cycle, followed by renewed burial during a later orogeny. Since the mesoscopic-scale folds correspond to shears that interfere in low strain zones, the structural pattern represents heterogeneous, rather than homogeneous strain accommodation during mid-crustal deformation.

Keywords: Angul Domain; Eastern Ghats; Mid-crustal reworking; Granulites; P-T path

1. Introduction

Orogenic belts are inherently susceptible to reactivation and rifting (e.g. Ring, 1994; Vauchez et al., 1997), and can evolve into passive margins that form locales of future continent-continent collision (Krabbendam, 2001). As a consequence, present-day continental margins can preserve crust that has been 'reworked' in earlier tectonic cycles. Within Precambrian shields, ancient terrane margins have in places been identified as collisional sites (e.g. Roering et al., 1992; Gupta et al., 2000), and by analogy, may preserve evidence of older orogenies. However, terrane margins normally expose deep crustal sections, where reworking involves the repeated focusing of metamorphism, deformation and magmatism into the same crustal- or lithospheric-scale volume (Holdsworth et al., 2001). This results in the elimination or re-equilibration of older mineral assemblages, resetting of isotope systematics, and transposition of older structures and fabric elements into an orientation sympathetic with the trend of the new orogen. Recognition of earlier tectonic events is therefore only possible in cases where the above processes do not proceed to completion.

In India, the Eastern Ghats Belt (EGB) is a granulite facies terrane that was reportedly amalgamated to the rest of the Indian craton (Fig. 1) in Proterozoic to early Phanerozoic time (Mezger and Cosca, 1999; Upadhyay et al., 2006; Dobmeier et al., 2006). A major part of the belt, designated as

* Corresponding author. Fax: +91 3222 255 303.
E-mail address: saibl@gg.iitkgp.ernet.in (S. Gupta).

0191-8141/$ - see front matter © 2007 Elsevier Ltd. All rights reserved.
doi:10.1016/j.jsg.2007.01.005

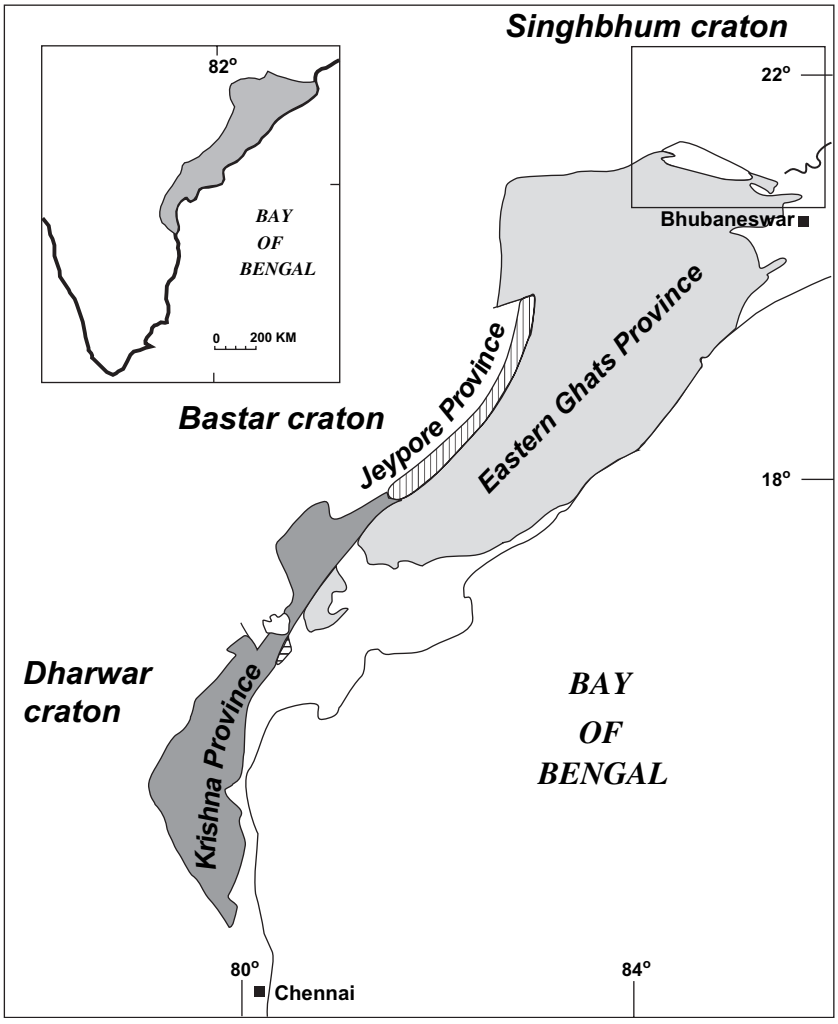

Fig. 1. Simplified classification of the Eastern Ghats Belt (see inset), after Dobmeier and Raith (2003). The Eastern Ghats Province is juxtaposed against the Archaean Jeypore Province and Bastar craton to the west, and the Singhbhum craton to the north. The rectangular area is the part enlarged in Fig. 2.

the Eastern Ghats Province (EGP; Dobmeier and Raith, 2003), preserves a penetrative NE-SW to N-S trending fabric (Naqvi and Rogers, 1987; Chetty and Murthy, 1998), and experienced high grade metamorphism of Late Mesoproterozoic, i.e. Grenvillian age (960–920 Ma; Aftalion et al., 1988; Mezger and Cosca, 1999). The granulites were reworked and exhumed following a later Late Neoproterozoic-Cambrian (i.e. Pan-African, ~500 Ma) thermal event (Mezger and Cosca, 1999) recorded across most of the province. The northern part of the terrane, referred to as the 'Angul Domain' (Dobmeier and Raith, 2003; Fig. 2), is characterized by a swing in structural trends that is evident on regional-scale lineament maps (Mahalik, 1996; Nash et al., 1996; Chetty and Murthy, 1998). In addition, the northern EGP also preserves thermal imprints at ca. 850 Ma (Halden et al., 1982; Lisker and Fachmann, 2001), and ca. 700–650 Ma (Crowe et al., 2001; Dobmeier and Simmat, 2002) intermediate between the Late Mesoproterozoic and Late Neoproterozoic-Cambrian events.

This paper describes the structural pattern and deformation history of a part of the Angul Domain, and discusses the significance of the swing in structural trends and radiometric ages in the context of the geological history of the Eastern Ghats Province. We demonstrate that the structural trends in this region result from reworking of the northern margin of the belt under mid-crustal conditions, during a later tectonic event. The documented structural pattern sheds light on the manner in which the middle crust responds to deformation in general, and may explain the deformation pattern observed in many amphibolite facies gneisses that dominate Precambrian shield areas.

2. Geological background

The intensely deformed granulites of the EGB include a variety of metasedimentary units and intrusive igneous rocks (e.g. charnockites, anorthosites, megacrystic granitoids and alkaline intrusives) enclosed within migmatitic quartzofeldspathic gneisses (see Ramakrishnan et al., 1998). Northeast-southwest trending foliations dominate the structural grain of the belt (Naqvi and Rogers, 1987; Chetty and Murthy, 1998). In much of the EGB Archaean to Mesoproterozoic crust was affected by Late Mesoproterozoic high grade

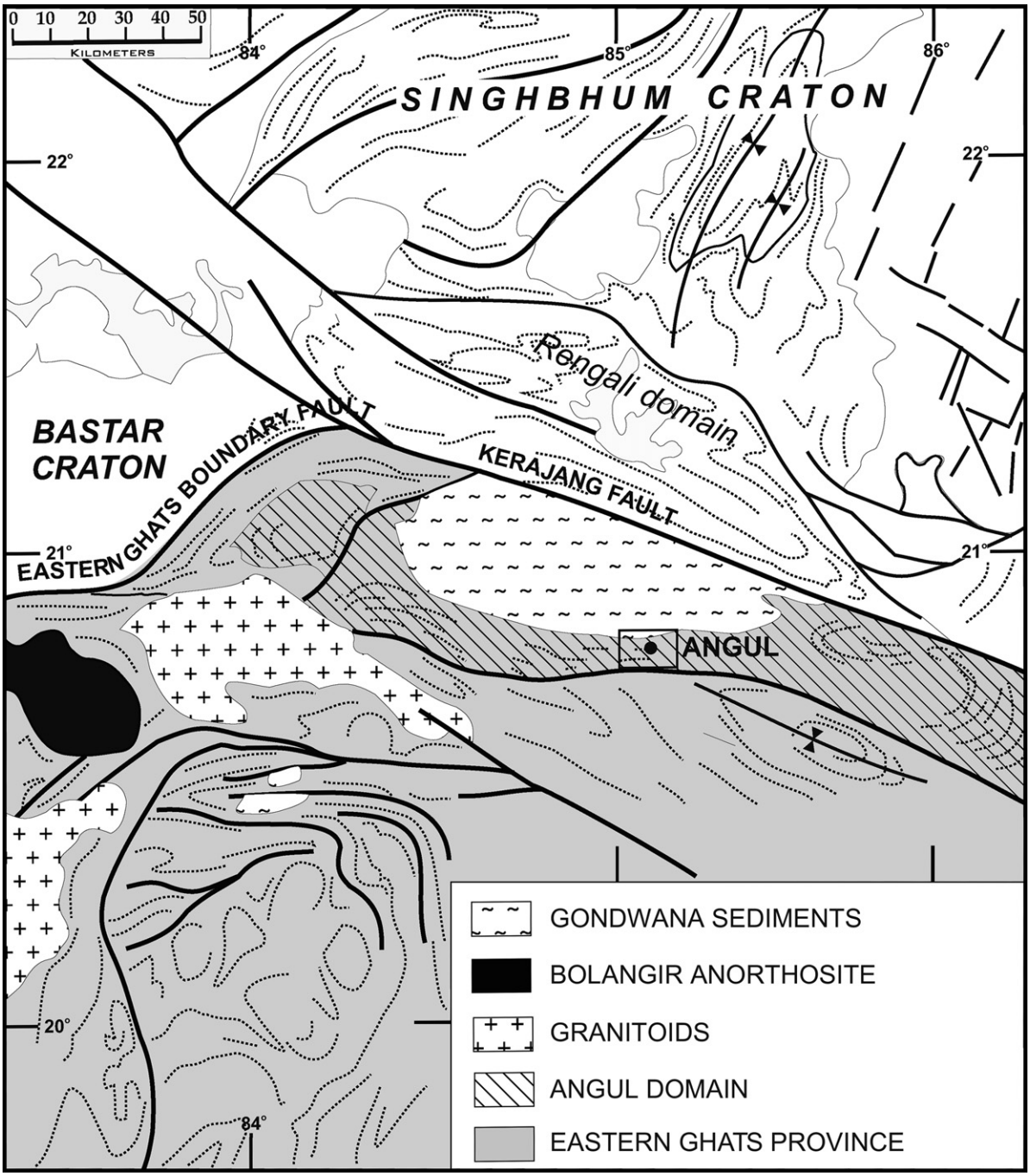

Fig. 2. Lineament map of the northern part of the Eastern Ghats Province (shaded) after Nash et al. (1996). The province is separated from the Bastar craton by the Eastern Ghats Boundary Fault, and from the Singhbhum craton by the Kerajang Fault. Note that dominant lineament trends in the Angul Domain (hatched) trend WNW-ESE and E-W, parallel to the Rengali Domain immediately north of the fault. The rectangular block around Angul town demarcates the present study area.

metamorphism (Rickers et al., 2001); this region was classified as the Eastern Ghats Province (EGP) by Dobmeier and Raith (2003). This age was related to an orogenic event that simultaneously affected a contiguous Proterozoic entity that included the EGB of India and the Rayner Complex of East Antarctica (Aftalion et al., 1988; Mezger and Cosca, 1999; Boger et al., 2001; Fitzsimons, 2003). Structural and petrological studies have interpreted the contact between the EGB and the Indian craton as a suture zone (Gupta et al., 2000). The Late Neoproterozoic-Cambrian thermal event (Mezger and Cosca, 1999) has been correlated with a separate orogeny involving the western front of the EGB and the Dharwar and Bastar cratons (Fig. 1.; Bhadra et al., 2004; Gupta, 2004; Upadhyay et al., 2006; Dobmeier et al., 2006). In the north, the EGB is separated from the Singhbhum craton by a distinct lithological, structural and metamorphic belt known as the Rengali Province (Crowe et al., 2003), but the precise nature of this contact is uncertain.

Lineament studies indicate that the dominant structural trend in the Angul Domain is predominantly WNW-ESE

(Mahalik, 1996; Nash et al., 1996; Fig. 2), unlike the NE-SW trends in the rest of the EGP (Chetty and Murthy, 1998). Mahalik (1994, 1996) correlated these trends with structures in the Singhbhum craton to the north. Specifically in the Angul area, Halden et al. (1982) describe a variety of quartzofeldspathic gneisses with a complex structural history comprising four deformation phases and concomitant migmatisation. North of Angul town, bands of garnet-sillimanite gneisses and schists, quartzites, calc-silicate granulites, and charnockite group rocks are locally traceable. Basic rocks include mafic granulites that occur as boudins within metapelites, calc-silicates and gneisses, and dykes (now amphibolites) that cut across the dominant regional fabric. Granitic rocks with graphic intergrowth textures and pegmatites are late and intrude the entire lithologic milieu. In the rest of the area, these lithologies occur sporadically and are not traceable on map scale. There is little published information on the metamorphic assemblages or their P-T conditions, although the limited petrological information available (e.g. Bhattacharya and De, 1969; Gupta et al., 2005) suggests similarity with assemblages in similar lithologies in the rest of the province.

3. Structural pattern

In the study area around Angul, planar units that act as marker horizons are not regionally traceable. Competent lithologies within the host quartzofeldspathic gneisses, such as calc-silicates, metapelites and mafic granulites, are boudinaged in the course of penetrative deformation and consequently no longer form continuous bands. Additionally, the primary depositional surface (S_0) is only rarely preserved (as colour bands in quartzites, and along quartzite-metapelite interfaces) and therefore cannot serve as a marker plane. On the other hand, the penetrative planar fabric, S_1, formed as a result of the first deformation event D_1, occurs in a wide variety of rocks, and is parallel to S_0 when both occur together. Under these circumstances, the regional structural pattern is best reconstructed from the disposition of the S_1 fabric in the area. The structural evolution subsequent to D_1 can be determined from the geometry of this fabric consequent to successive deformation events.

In the area mapped during the present study (Fig. 3), form surfaces following the trend of the S_1 fabric are also incidentally parallel to regional topographic features. In the west, S_1 form surfaces show consistent WNW-ESE trends, in accordance with regional lineament patterns (Nash et al., 1996; Fig. 2). In the central part of Fig. 3, these trends are deflected around a core dominated by meta-sedimentary and igneous lithologies, and foliation trend lines become distinctly curved indicating swerving of the S_1 fabric. Evidence for regional-scale superposed deformation is preserved north of Angul town, where a Type 3 interference pattern (Ramsay, 1967) characteristic of collinear refolding is mimicked by impersistent metasedimentary and igneous bands. However, the equal area plot of poles to S_1 over the whole area (Fig. 4a) shows a strongly non-cylindrical distribution; this cannot be explained by collinear refolding, and indicates a considerably more complicated history. The contoured foliation plot distribution also reveals three submaxima whose significance is discussed later.

The heterogeneous structural pattern and non-cylindrical distribution of the S_1 foliation may indicate either polyphase deformation or sheath folding of the S_1 fabric. The control has been established by systematic unravelling of the deformation history of the area following detailed mapping and structural analysis of fold interference patterns on outcrop-scale. These observations have then been extrapolated to regional-scale, as suggested by Hopgood (1999).

4. The deformation sequence

S_1 has been deformed by a succession of four deformation events (D_2 to D_5). D_2 involves shearing and isoclinal folding that form part of a single sequence. Mafic dyke intrusion occurred during extensional deformation, D_3; further uplift occurred during a non-penetrative shearing event (D_4) that was accompanied and outlasted by the intrusion of granite magma and pegmatite. A final phase of deformation, D_5, obliterated most evidence of earlier deformation, except in localities in the vicinity of Angul town. In conjunction with the metamorphic evolution, it is argued that the later D_5 event represents a separate tectonic cycle.

4.1. D_1 deformation

The earliest detectable deformation event, D_1, is characterized by a penetrative compositional segregation banding (S_1). S_1 is observed in nearly all lithologies. In migmatised quartzofeldspathic gneisses that comprise the country rock, S_1 is defined by the segregation of biotite, garnet, opaques and occasionally, orthopyroxene into discrete mafic bands. Commonly, the banding is further accentuated by the segregation of leucocratic components parallel to S_1. In garnet-sillimanite gneisses, the foliation is defined by alternating felsic (quartzofeldspathic) and garnet + sillimanite bearing mesocratic layers. S_1 is also prominent in augen-gneisses, where felsic layers of quartz and aligned porphyroclasts of alkali feldspar alternate with biotite + garnet-bearing mafic layers. In enderbites, on the other hand, S_1 is characterized by plagioclase-rich layers that alternate with orthopyroxene + clinopyroxene + garnet-rich layers.

Cross-cutting relationships between S_0 and S_1 have not been observed, but S_1 is never associated with primary sedimentary structures. Further, S_1 in metasedimentary rocks is invariably parallel to the early compositional layering in igneous lithologies (e.g. augen gneisses and charnockites). This reinforces the conclusion that S_1 is not a primary sedimentary layering and is related to penetrative deformation (D_1).

4.2. D_2 deformation

A second penetrative deformation event D_2 affected all pre- to syn-D_1 lithologies, and is manifested either as isoclinal folding or penetrative shearing on S_1. In garnet-sillimanite

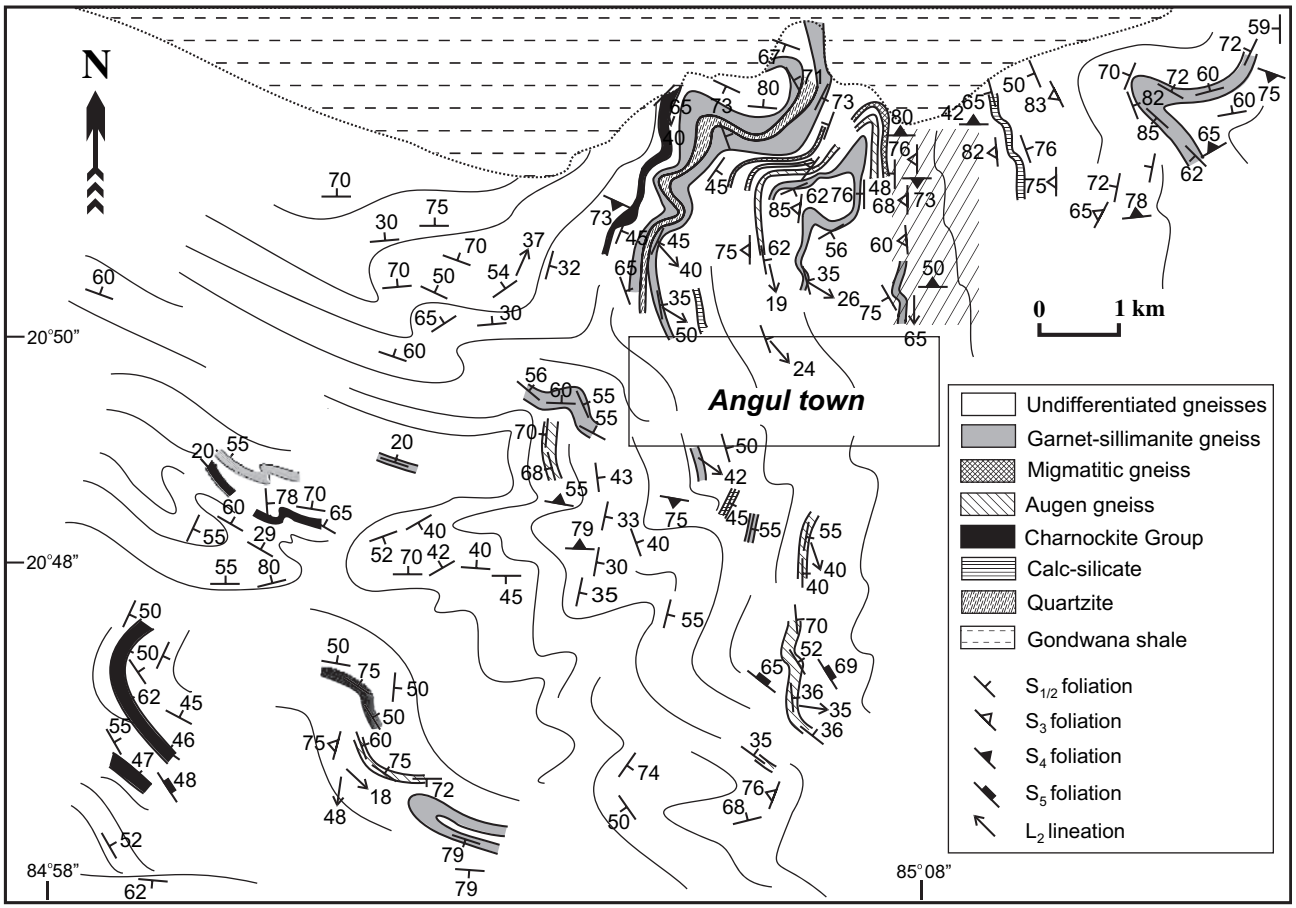

Fig. 3. Geological map of the study area that comprises quartzofeldspathic gneiss along with distended metasedimentary and metaigneous bands. In the absence of continuous marker horizons, structural trends are demarcated by form surfaces that follow the S_1/S_2 foliation in the gneiss and other lithologies. Note that the WNW-ESE trend in the western part of the map is deflected in the central and northeastern part of the map. The rectangular block demarcates the approximate limits of Angul town. Hatched area northeast of the town represents D_3 shear zone.

gneisses and augen gneisses D_2 is characterized by a progressive sequence of isoclinal folding (F_{2A}) and open to tight refolding (F_{2B}) of S_1 about collinear axes. Regional scale F_{2A} isoclinal folds are preserved north of Angul town (Fig. 3). More commonly, F_{2A} folds are mesoscopic, with an associated penetrative axial planar schistosity (S_{2A}). These folds are always isoclinal and almost invariably reclined. The S_{2A} schistosity in garnet-sillimanite gneisses is defined by recrystallized sillimanite-rich surfaces; the S_1/S_{2A} intersection lineation (δ_2) parallels F_2 fold axes and is also characterized by aligned sillimanite needles (L_2). L_2/δ_2 lineations show a spread, but with a southwesterly plunging maxima (Fig. 4b). Subsequently, S_{2A} is openly refolded (F_{2B}) along axes parallel to F_{2A}. Interference of F_{2A} and F_{2B} folds gives rise to Type 3 interference patterns, typical of interfering folds with collinear axes. These relationships are demonstrable on outcrop-scale within the garnet-sillimanite gneisses (Fig. 5a). In these domains the L_2 lineation forms a southwesterly plunging cluster (plot in Fig. 5a), with no spread consistent with the collinear nature of refolding. The cluster coincides with the maxima in Fig. 4b.

In parts of the migmatised country rock, and other lithologies such as the migmatised gneiss band and calc-silicates, the D_2 deformation is manifested in the form of penetrative shearing. The shearing is pervasive and leads to near-complete transposition of the S_1 compositional layering; in all cases, S_2 shear planes define the outcrop trend. In domains of high D_2 strain, S_1 and S_2 are indistinguishable; however, extensively folded and partially rotated S_1 layers can be seen curving into the S_2 shear planes with a predominantly dextral sense (Fig. 5b). The intrafolial S_1 folds vary from closed to isoclinal, with axial planes sub-parallel to the bounding S_2 shears. Poles to these S_1 layers (Fig. 5c) define a girdle comparable to that in Fig. 5a. In sections normal to the S_2 shears, and parallel to the southerly plunging δ_2 lineation, the shear sense is invariably top-to-the-north (Fig. 5d). The gneisses also frequently contain boudins of mafic granulite, some of which describe Type-3 interference patterns due to superposition of collinear F_{2A} and F_{2B} folds (Fig. 5e). The evidence suggests that penetrative folding and shearing on S_1 are intrinsically related to the D_2 deformation.

Parts of the study area where S_1 foliation poles retain a cylindrical distribution, and all D_2 lineations show point clustering about southwesterly plunges, are interpreted to have experienced limited post-D_2 strain, implying widespread strain partitioning during subsequent deformation. Overall, the

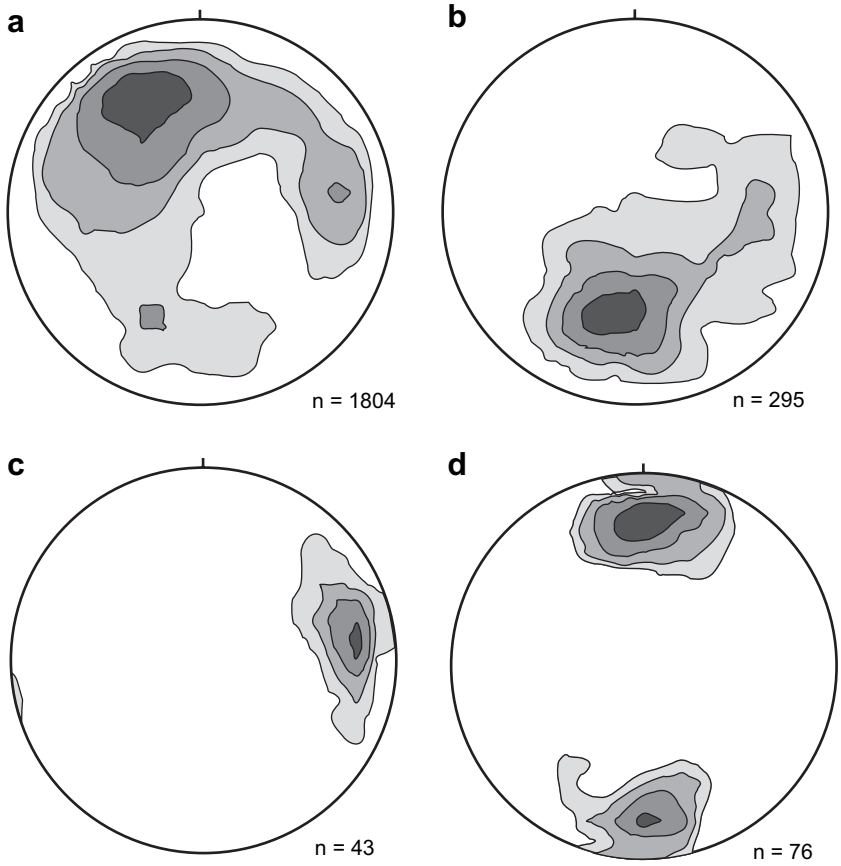

Fig. 4. Stereographic projection of structural elements in the study area. (a) Equal area plot of poles to the S_1 foliation in all rock types, contoured at intervals of 1%, 2%, 4% and 8%. Note the absence of cylindricity in the foliation distribution, and the three submaxima around 242°/55°E, 172°/62°W and 114°/40°S. (b) Plot of the L_2/δ_2 lineation in all lithologies contoured at intervals of 1%, 4%, 8% and 16%. The distribution reflects rotation from a mean value of 47°/191° to 36°/080°, and can be approximated by a girdle oriented 233°/33°W. (c) Equal area plot of poles to the S_3 foliation in all rock types, contoured at intervals of 3%, 12%, 24% and 48%, with a preferred direction of 169°/69°W. Note that this correlates with submaxima in the S_1 foliation plot. (d) Equal area plot of poles to the S_4 foliation in all rock types, contoured at intervals of 2%, 4%, 8% and 16%.

D_2 deformation event can be regarded as a continuum involving F_{2A} and F_{2B} folding, and shearing along ENE-WSW trending, southerly dipping planes. The association of widespread reclined folding with top-to-the-north shearing on south-dipping S_2 shear planes, and the parallelism of the L_2 and δ_2 lineations, suggests that D_2 was predominantly thrust-related deformation associated high shearing parallel to L_2/δ_2.

4.3. D_3 deformation

The D_2 deformation was followed by the intrusion of mafic dykes that are now metamorphosed to amphibolites (Fig. 6a). Unlike the mafic granulites that are conformable with the S_1/S_2 layering, these dykes are not boudinaged and cut across the penetrative foliation. The dykes vary from several centimetres to over 2 metres in thickness, and in most parts of the area, are oriented north-south, except in the vicinity of D_5 shear zones where they may be substantially reoriented. The dykes are interpreted to represent the onset of a phase of extensional deformation, D_3.

The most prominent manifestation of D_3 deformation occurs to the northeast of Angul town (Fig. 3), where a north-south trending, westerly dipping shear zone (D_3) intersects the country rocks and persists along strike for over 2 km. In the vicinity of the shear zone, the S_1 and S_2 foliations within the migmatitic gneisses are initially reoriented, and then replaced by a new fabric parallel to the S_3 shears. Poles to S_3 shear planes across the area (Fig. 4c) describe a cluster that correlates with one of the submaxima in the S_1 foliation plot (Fig. 4a). This testifies to reorientation of the S_1 foliation in the vicinity of S_3 shear planes. On the S_3 shear plane, a down-dip lineation defined by elongate quartz grains is locally observed, and is inferred to represent the movement direction (Fig. 6c). In calc-silicate bands within the shear zone (see north-eastern corner of Fig. 3), S_1 is reoriented into a new S_3 fabric; in sections normal to the west-dipping S_3 foliation and parallel to the down-dip lineation, the shear sense is top-to-the-west (Fig. 6b). D_3, therefore, extended the crust, as there is no evidence for reorientation of this S_3 shear plane by subsequent deformation.

Away from the shear zone, mesoscopic manifestations of this deformation are limited. Occasionally, ~10 cm wide D_3 shear zones intersect the S_1/S_2 foliation, particularly in N-S trending, easterly-dipping metapelite and charnockite bands

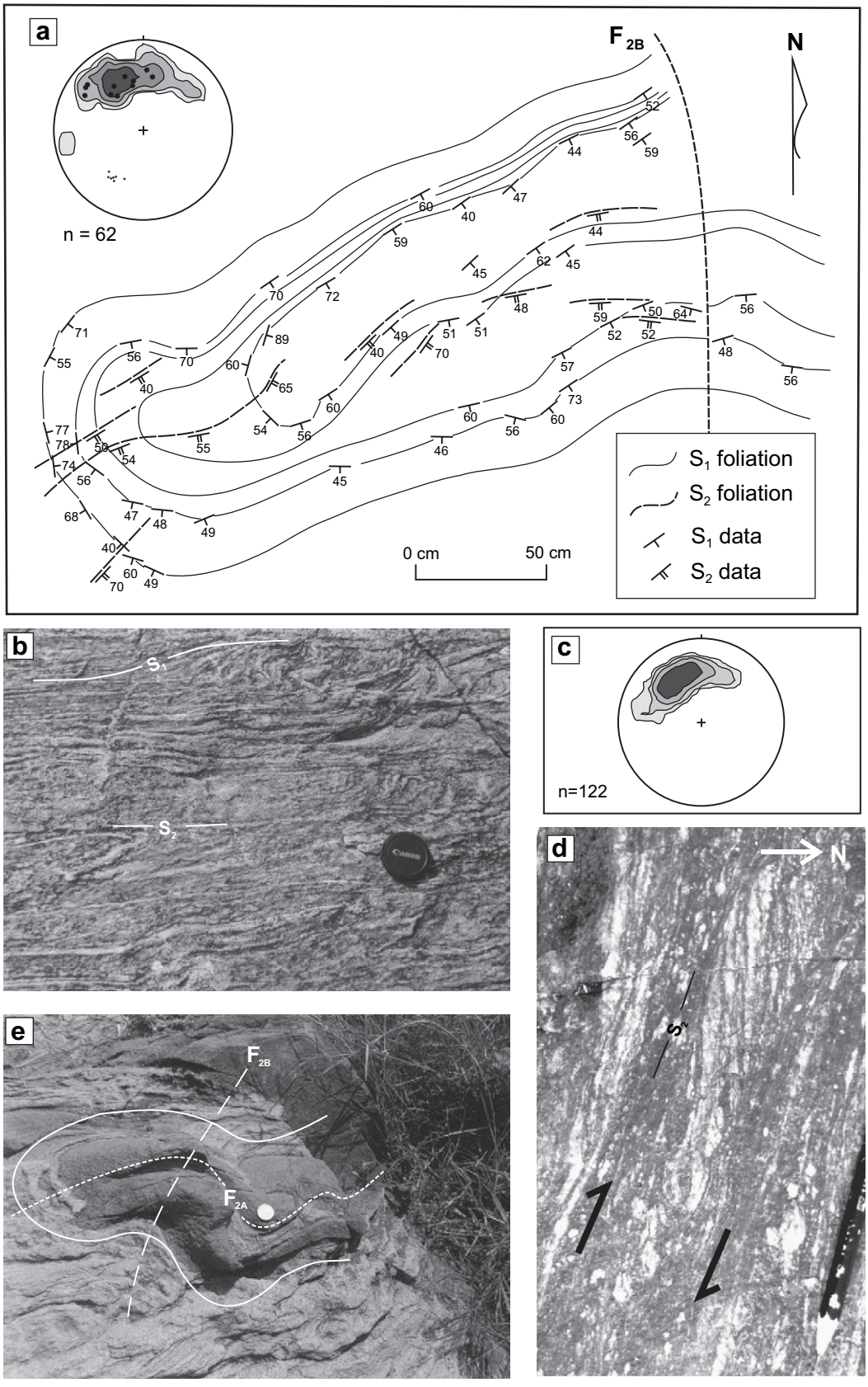

Fig. 5. D_2 deformation in region unaffected by post-D_2 strain. S_2 is dominantly oriented NE-SW, and dips to the southeast, comparable to the one of the submaxima in the regional S_1 foliation plot. (a) Outcrop map of F_{2A} isoclinal fold refolded (F_{2B}) into a Type 3 interference pattern in garnet-sillimanite gneiss. The S_1 gneissic layering (contoured at 2%, 4%, 8% and 16%) and S_2 axial planar fabric (larger dots) show identical distributions characteristic of collinear folding. The L_2 lineation data (smaller dots) clusters around 47°/191°. (b) Folded and rotated S_1 layers preserved between S_2 shear planes in migmatitic gneiss band. (c) Contoured equal area plot (at 2%, 4%, 8% and 16%) of S_1 gneissic layering intrafolial to S_2 shear planes in Fig. 5b. Note similarity of the girdle distribution with that for S_1 in the outcrop map of the isoclinal fold. (d) Section normal to S_2, parallel to δ_2 lineation in migmatitic gneiss, showing top-to-the-north sense of shearing. (e) Mafic granulite boudin in migmatitic gneiss band shows Type 3 interference pattern due to superposition of collinear F_{2A} and F_{2B} folds.

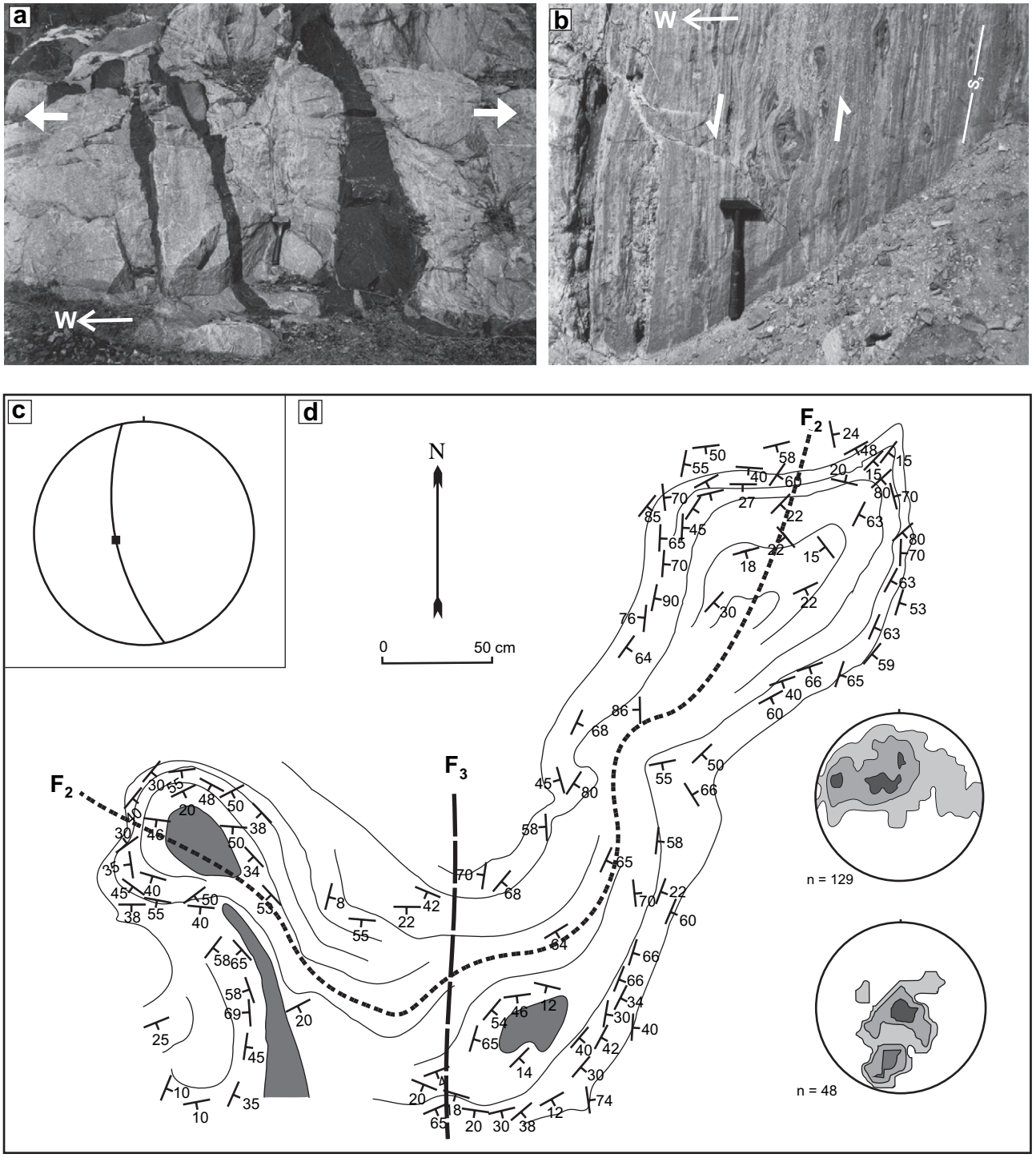

Fig. 6. D_3 deformation. (a) North-south trending mafic dykes intrude augen-gneiss at the outset of D_3 extension. These dykes are now metamorphosed to amphibolites. (b) Vertical section parallel to mineral lineation defined by elongate quartz grains in calc-silicate gneiss, showing transposition of the S_1 fabric into a new S_3 fabric within D_3 shear zone. Note that hornblende rich mafic segregations show asymmetric lenticular shapes within the shear zone, and indicate down-dip movement sense. (c) Average orientation of the S_3 shear plane (169°/69°W), with down-dip lineation (filled square). (d) Outcrop map showing the superposition of F_3 fold warp on F_{2A} isoclinal fold, to define a Type 2 interference pattern. Note that the axial trace of the F_3 fold parallels the trend of the S_3 shear plane in garnet-sillimanite gneiss. The S_1 gneissic layering (contoured at 1%, 4% and 8%) shows a non-cylindrical distribution, and the δ_2 lineation (contoured at 3%, 6% and 12%) show a corresponding scatter.

northwest of the Angul town. These result in the formation of a series of N-S trending non-plunging folds and warps on the early fabric, and also interfere with later WNW-ESE trending D_5 warps to form Type 1 interference structures on the dominantly easterly dipping S_1 foliation. In the vicinity of (but not adjacent to) D_3 shears, F_3 fold warps with N-S trending axial planes interfere with F_{2A} isoclinal folds to form typical Type 2 interference patterns (Fig. 6d). These warps represent the first significant contribution to the non-cylindrical distribution of the S_1 fabric and the δ_2 lineation on a regional scale (Fig. 6d).

4.4. D_4 deformation

E-W trending shears that dip steeply either towards north or south, occur sporadically throughout the area (Fig. 4d). The shears generally occur in clusters of spaced parallel planes, with individual shears varying from a few centimetres to half a metre in thickness. The narrower zones can be identified as discrete shear planes (S_4) that displace S_1/S_2 and S_3 within the D_3 shear zone; the wider shears form warps with E-W trending axes on the S_1/S_2 foliation. Vertical sections reflecting the precise nature of shear could not be observed, but in plan view, the apparent sense of displacement of the S_1/S_2 foliation is generally sinistral. On outcrop scale, S_4 shears cut across S_2 shear planes and F_{2A} and F_{2B} folds on the S_1 foliation (Fig. 7a), but cause no reorientation of either the earlier fold axes or the related foliations. Even within the D_3 shear zone, displacement of S_3 is only observed within a few centimetres of the S_4 shears (Fig. 7b). This suggests that rotation or transposition of earlier fabrics during D_4 is minimal, and that regional-scale deflection of the penetrative fabric cannot be attributed to this deformation.

S_4 planes that cut across syn-D_3 mafic dykes form conduits for the migration of very coarse-grained tourmaline-bearing biotite granitoids (Fig. 7c) and fine-grained aplites (Fig. 7d). The coarse-grained granitoids eventually grade into pegmatites that contain quartz, muscovite, biotite, K-feldspar, plagioclase and tourmaline. Unfortunately, no lineation was observed associated with the S_4 shear planes, and therefore, the precise movement sense remains undetermined. However, regional-scale fabric transposition is relatively unimportant; consequently, none of the S_1 foliation submaxima (Fig. 4a) coincide with the subvertical S_4 shear clusters (Fig. 4d). D_4 is therefore characterized by the segregation of syntectonic granitic and pegmatitic melts, but little regional-scale fabric reorientation.

4.5. D_5 deformation

S_4 shears (and associated melts) that displace earlier S_1/S_2 and S_3 fabrics are themselves truncated by later WNW-ESE trending shears that dip to the north (Fig. 7e). Unlike D_4 shears, these late (S_5) shears cause considerable reorientation of earlier fabrics, and are correlated with a distinct deformation event D_5. S_5 shear planes are rare, but the D_5 deformation results in regional-scale transposition of the S_1/S_2 foliation into a WNW-ESE, north dipping orientation. In the proximity of high D_5 strain zones, warps appear on the S_1 foliation that interfere with earlier folds. As in the case of D_3, axial traces of F_5 warps parallel the trend of S_5 shear planes. Biotites in syn-D_4 melts are frequently kinked during the D_5 event, while quartz within the melts is typically strained and tends to wrap around feldspars and biotites near D_5 shears.

West and south of Angul town, topographic features parallel the WNW-ESE trend of D_5 shearing. Within this zone there is intense realignment of the S_1/S_2 foliation parallel to the trend of the D_5 shear plane. As the S_1/S_2 foliation swings from the typical D_2-related, NE-SW trending, south-easterly dipping orientation (see maxima in Fig. 5a,c) into the D_5 trend, warps related to D_5 shearing are superposed on the gneiss outcrops within this zone (Fig. 8a). Foliation poles in such outcrops describe a girdle distribution that reflects rotation of the foliation from the average D_2 to the average D_5 trend. The presence of minor F_{2A} folds (as in Fig. 8a) results in the development of incomplete Type 2 interference patterns; this demonstrates how the regional S_1 foliation pole distribution becomes non-cylindrical as a result of interference.

No linear fabric element could be identified to be associated with the D_5 shear planes. However, in the zones where the S_1/S_2 foliation is reoriented parallel to the D_5 shear, the S_1/S_2 intersection lineation (δ_2) clusters in a more easterly orientation (Fig. 8b). In vertical sections through the S_5 shear plane, sub-parallel to this lineation, the S_1/S_2 fabric is displaced and shows a clear top-to-the-south shear sense (Fig. 7f). The shallow easterly plunging δ_2 lineation maximum is therefore considered to approximate the movement direction on the S_5 shear plane. Together with the observed top-to-the-south shear sense, this indicates thrusting and loading associated with a significant strike-slip component during the D_5 deformation event. The apparent reorientation of the δ_2 lineation in D_5 shear zones is best interpreted in terms of the rotation of passive linear markers towards the movement direction as a consequence of shear deformation (Ramsay, 1967; Wheeler, 1987). This also effectively explains the dispersion of the L_2/δ_2 lineation on a regional scale (Fig. 4b), from an original southwesterly orientation (Fig. 5a) to the rotated position following D_5 deformation (Fig. 8b).

5. Metamorphism and deformation

The S_1 segregation banding and S_2 shear planes are defined by mineral assemblages that characterize granulite facies conditions. In addition, orthopyroxene-bearing syn-D_1 and syn-D_2 leucosomes bear testimony to the high metamorphic grade (granulite facies) accompanying D_1 and D_2 deformation. High grade conditions persisted after D_2, with garnet-orthopyroxene-clinopyroxene-plagioclase assemblages in mafic granulites and scapolite-anorthite-calcite association in calc-silicates (Fig. 9a) forming granoblastic mosaic textures that overgrow F_2 isoclinal fold hinges. The peak of granulite facies metamorphism (M1) therefore followed the D_2 deformation event.

The metamorphic grade during D_3 deformation is less obvious. Fabrics in quartzofeldspathic gneisses of the D_3 shear

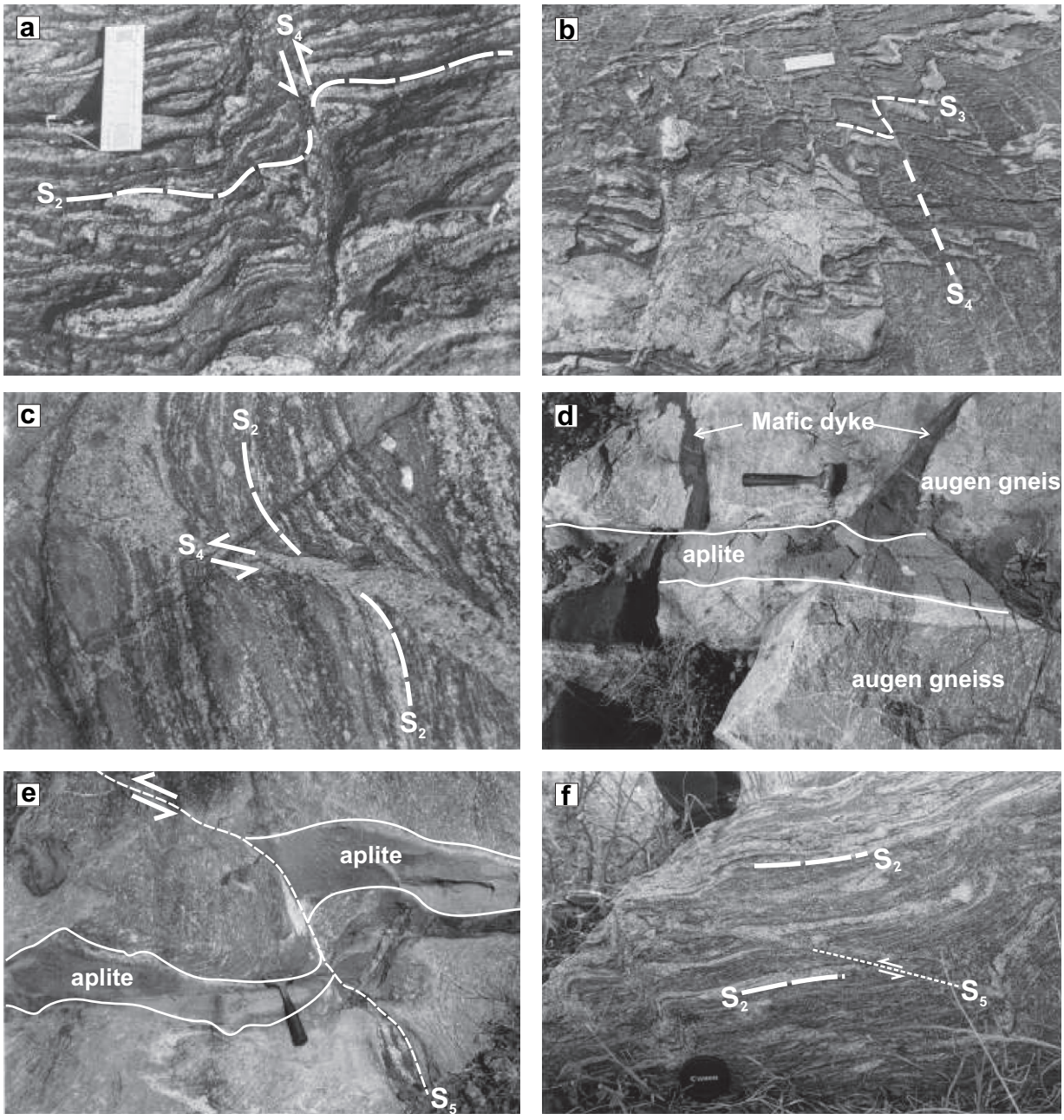

Fig. 7. Field photographs showing (a) sinistral displacement of the S_2 foliation across narrow S_4 shear plane, migmatitic gneiss band. (b) Sinistral displacement of the S_3 foliation by S_4 shear plane, migmatitic gneiss band. (c) Segregation of granitic melt along D_4 shear plane in quartzofeldspathic gneiss (d) N-S trending syn-D_3 mafic dykes truncated by aplitic melts segregated along D_4 shear planes. (e) Syn-D_4 aplite dyke sinistrally displaced by S_5 shear plane. (f) Thrust-sense displacement of S_2 fabric along S_5 shear plane, parallel to the easterly plunging δ_2 lineation (39°/90°) that is inferred to represent the movement direction (length of diagonal scale 15 cm, hammer 30 cm). Vertical N-S section, facing west.

zone show stabilization of amphibole and biotite, possibly at the expense of pyroxene; likewise, syn-D_3 mafic dykes preserve an amphibolite facies mineralogy. Garnets within mafic granulites decompose to symplectitic intergrowths of orthopyroxene and plagioclase (Fig. 9b), textures generally associated with high temperature decompression. These are compatible with the extensional sense inferred for the D_3 deformation event.

While there is no direct indication of the grade of metamorphism associated with D_4, the presence of the assemblage muscovite + quartz in the associated melts indicates metamorphic conditions within the muscovite stability range (i.e., middle amphibolite facies conditions). This is consistent with continuing uplift from higher pressures after the M1 peak.

Following D_5, garnets form along amphibole-plagioclase interfaces in amphibolites (Fig. 9c), and along biotite-plagioclase ± quartz interfaces within coarse D_4 granitic melts (Fig. 9d). Simultaneously, in mafic granulites, renewed garnet formation occurs along orthopyroxene-plagioclase interfaces in syn-D_3 symplectites (Fig. 9b). Together, the evidence

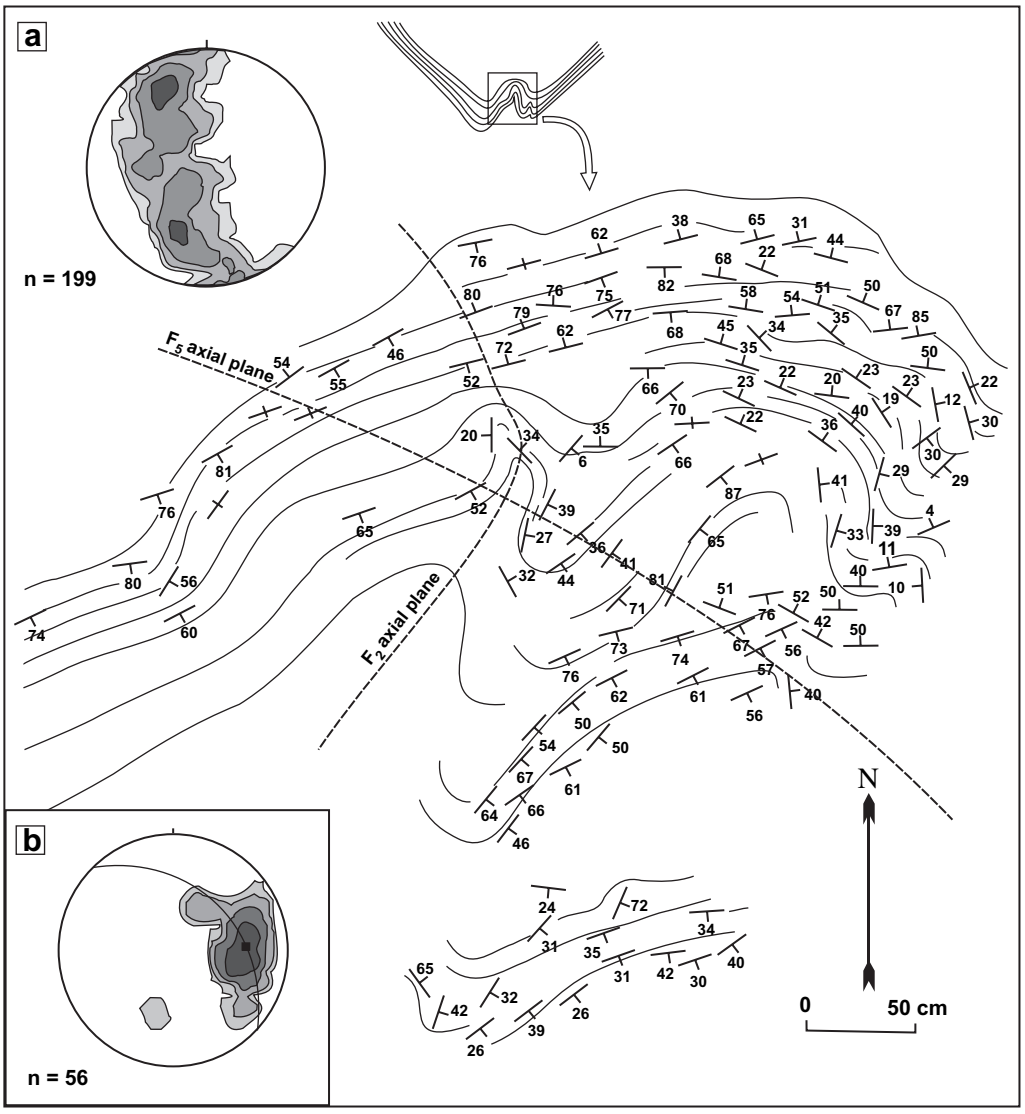

Fig. 8. (a) Outcrop map showing incomplete Type 2 interference pattern between minor F_{2A} folds on the S_1 foliation and D_5-related warps (S_1 plot contoured at 1%, 2%, 4% and 8%). Immediately southwest of this outcrop, the foliation is consistently oriented at 135°/45°E. (b) Plots of δ_2 lineation in regions where S_1/S_2 is transposed into a WNW-ESE orientation (plot contoured at 2%, 4%, 8% and 16%). Note that the distribution resembles an imperfect point cluster around an average orientation (marked as filled square) that plunges east (39°/90°). Girdle represents S_5 (135°/45°E).

suggests a second phase of metamorphism (M2) following the D_4 and D_5 deformation events.

5.1. Pressure-temperature conditions during metamorphism

Pressure-temperature conditions prevailing during M1 and M2 were estimated on the basis of the textural observations made in the relevant assemblages. Mineral chemical analyses were acquired on a CAMECA SX-51 electron probe microanalyzer at the Geological Survey of India, Faridabad. The operating conditions were: accelerating voltage – 15 kV, beam current – 12 nA, beam diameter – 1 μm. The PAP correction scheme was applied, and the data were calibrated against a set of natural standards. Mineral chemical analyses for phases used in the P-T calculations are given in Table 1.

Pressures and temperatures were estimated using a combination of conventional thermobarometers and the software THERMOCALC (v. 3.1), based on the internally consistent dataset of Holland and Powell (1998). Cation exchange thermometers in assemblages that stabilized during the early granulite facies event have largely re-equilibrated during later metamorphism, and uniformly yield temperatures compatible with M2 metamorphism. The best constraint on the early (i.e. M1) metamorphic temperature is from the scapolite-calcite-plagioclase assemblage in calc-silicate granulites that yield values of in excess of 750 °C (using THERMOCALC). Pressures during the M1 peak were estimated from the GRAIL barometer (Bohlen et al., 1983) in garnet-sillimanite gneisses, and are in the range of 7–8 kbars over a temperature range 600–800 °C. In garnet-sillimanite gneisses (Sample 42b) that preserve relatively undisturbed D_2 fabrics, temperatures

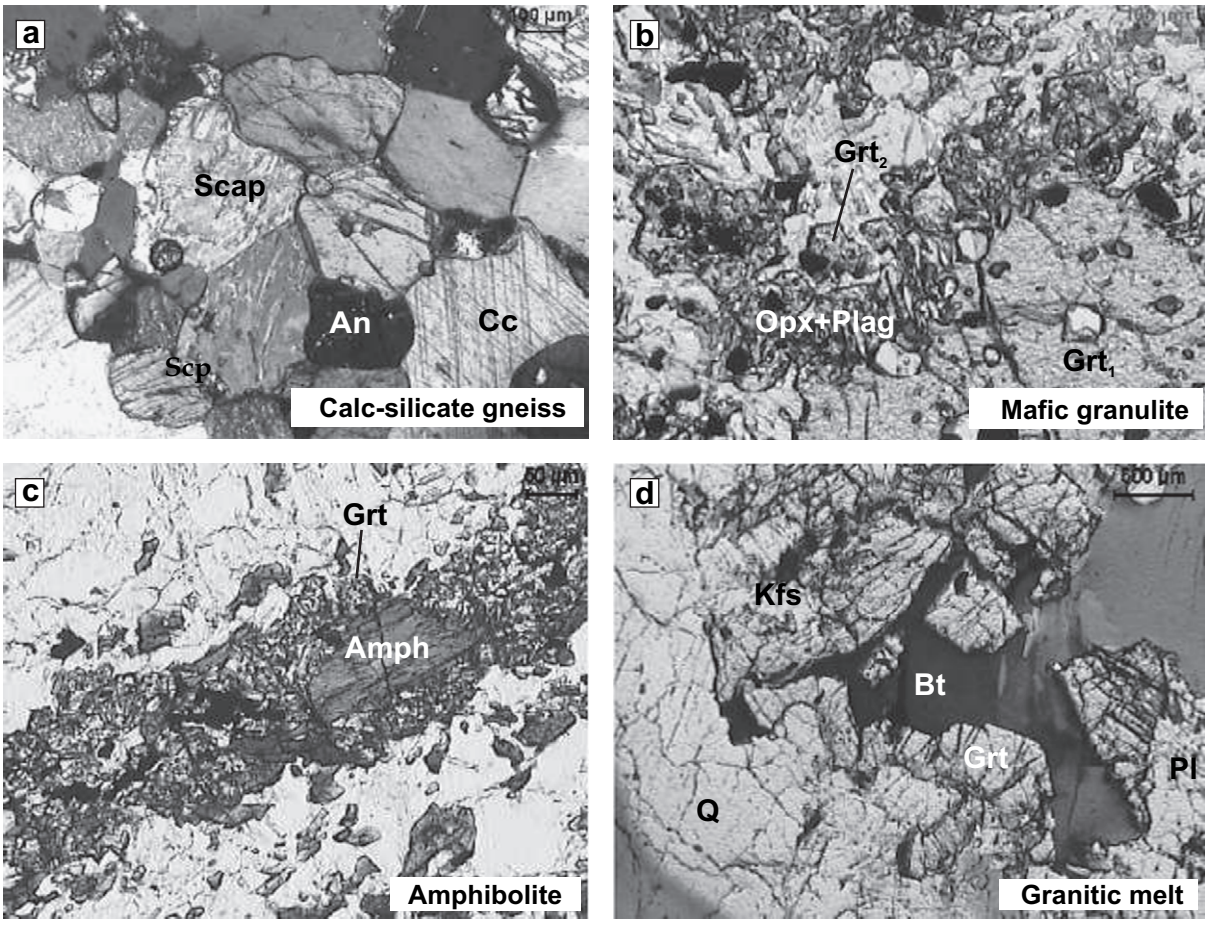

Fig. 9. Photomicrographs showing textural relations in various rock types. (a) Scapolite-anorthite-calcite assemblage defining a post-D_2 granoblastic assemblage in calc-silicate gneisses. (b) Marginal breakdown of porphyroblastic garnet (Grt_1) to syn-D_3 orthopyroxene + plagioclase symplectites in mafic granulite. The symplectite is overgrown by a second generation of garnet (Grt_2) following D_4 and D_5. (c) Post-D_4/D_5 coronal garnet overgrowing amphibole in syn-D_3 mafic dykes. (d) Post-D_4/D_5 garnet + K-feldspar forming along biotite − plagioclase + quartz interfaces in syn-D_4 granitic melts.

calculated from garnet-biotite pairs (Ferry and Spear, 1978) are lower (620–635 °C in the pressure range 5–8 kbars). Mafic granulites record temperatures of 552–565 °C (at 5–8 kbars, Harley, 1984) and pressures of ~4 kbars at these temperatures (Newton and Perkins, 1982) in calculations that use rim compositions of porphyroblastic post-D_2 garnets in conjunction with orthopyroxene and plagioclase in the adjacent symplectites. This reflects decompression and cooling of the terrane following the M1 granulite facies peak. Renewed garnet formation at the interface of orthopyroxene and plagioclase within the symplectite indicates reversal of the garnet breakdown reaction

$$\mathrm{Opx} + \mathrm{Pl} = \mathrm{Grt} + \mathrm{Q} \quad (1)$$

P-T calculations using THERMOCALC position the reaction as shown in Fig. 10, with a shallow positive slope. Stabilization of garnet can therefore take place either as a consequence of decreasing temperature or increasing pressure. Barometric calculations indicate higher pressures (~5.5 kbars; Newton and Perkins, 1982) for the new garnet-bearing assemblage, at equilibration temperatures of 618–633 °C (at 5–8 kbars, Harley, 1984), suggesting that reaction (1) was probably associated with increasing pressure. Garnet formation along amphibole-plagioclase contacts in amphibolite dykes is also consistent with increasing pressure (Ernst and Liu, 1998). The pressure-independent garnet-hornblende thermometer of Graham and Powell (1984) yields tightly constrained temperatures in the range 620–630 °C. Average P-T calculations in amphibolite Sample 77e using water independent runs suggests similar pressure-temperature ranges. Coincident P-T estimates in the amphibolite are obtained with $a_{H2O} = 0.25$, thereby constraining water activities during the M2 metamorphic event. Garnet formation in the late granitic melts can be represented by the reaction

$$2\mathrm{ann} + 3\mathrm{an} + 3\mathrm{q} = \mathrm{gr} + 2\mathrm{alm} + 2\mathrm{san} + 2\mathrm{H_2O} \quad (2)$$

This reaction has a very shallow negative slope (Fig. 10), and is consequently associated either with increasing temperature or increasing pressure.

Metamorphism in the post-D_2 period (M1) was therefore characterized by pressures of 7–8 kbars at temperatures greater than 750 °C. The late metamorphic episode (M2)

Table 1
Mineral chemical analyses of phases used in geothermobarometric calculations

Sample No.	ANG-79e						ANG-42b			ANG-84k		ANG-77e	
Rock Type	Mafic granulite						Metapelitic gneiss			Calc-silicate		Amphibolite	
	Garnet	Garnet	Opx	Cpx	Plag	Plag	Garnet	Biotite	Ilmenite	Scap	Plag	Garnet	Amph
	Symplec	Post-D_2	Symplec	Post-D_2	Symplec	Post-D_2	Post-D_2	Post-D_2	Post-D_2	Post-D_2	Post-D_2	Post-D_3	Post-D_3
SiO_2	36.87	36.84	50.54	52.31	45.14	44.47	38.11	35.75	0.00	43.93	43.44	37.09	39.81
TiO_2	0.02	0.00	0.05	0.02	0.00	0.00	0.00	4.81	53.34	0.00	0.00	0.01	1.60
Al_2O_3	21.21	21.36	0.60	0.76	34.90	35.83	21.76	16.69	0.03	29.35	35.71	20.18	12.22
Cr_2O_3	0.04	0.05	0.02	0.05	0.00	0.12	0.06	0.04	0.00	0.00	0.00	0.03	0.02
Fe_2O_3	3.07	3.06	1.77	1.28	0.08	0.59	0.05	0.00	0.00	0.00	0.02	2.02	0.38
FeO	26.19	29.40	29.88	10.34	0.00	0.00	34.18	15.93	45.66	0.10	0.00	28.99	24.41
MnO	1.45	1.59	0.36	0.10	0.01	0.02	0.90	0.00	0.12	0.11	0.00	1.58	0.08
MgO	3.59	3.41	16.54	12.20	0.00	0.02	4.95	11.50	0.58	0.01	0.01	0.86	4.41
CaO	7.81	5.36	0.59	23.06	18.42	19.21	1.17	0.00	0.01	20.60	19.41	9.45	11.47
Na_2O	0.01	0.02	0.00	0.18	1.28	0.67	0.02	0.15	0.02	2.31	0.57	0.02	1.57
K_2O	0.00	0.00	0.00	0.00	0.00	0.03	0.02	9.83	0.00	0.23	0.03	0.01	2.12
Total	100.26	101.10	100.35	100.31	99.83	100.96	101.23	94.71	99.76	96.78	99.19	100.24	98.09
Oxygen	12.00	12.00	6.00	6.00	8.00	8.00	12.00	11.00	3.00			12.00	23.00
Si	2.92	2.91	1.96	1.97	2.09	2.04	2.99	2.71	0.00	6.66	2.03	2.98	6.26
Ti	0.00	0.00	0.00	0.00	0.00	0.00	0.00	0.27	1.01	0.00	0.00	0.00	0.19
Al	1.98	1.99	0.03	0.03	1.90	1.94	2.01	1.49	0.00	5.24	1.97	1.91	2.27
Cr	0.00	0.00	0.00	0.00	0.00	0.00	0.00	0.00	0.00	0.00	0.00	0.00	0.00
Fe^{3+}	0.18	0.18	0.05	0.04	0.00	0.02	0.00	0.00	0.00	0.00	0.00	0.12	0.05
Fe^{2+}	1.73	1.95	0.97	0.33	0.00	0.00	2.25	1.01	0.96	0.01	0.00	1.95	3.21
Mn	0.10	0.11	0.01	0.00	0.00	0.00	0.06	0.00	0.00	0.01	0.00	0.11	0.01
Mg	0.42	0.40	0.96	0.69	0.00	0.00	0.58	1.30	0.02	0.00	0.00	0.10	1.03
Ca	0.66	0.45	0.03	0.93	0.91	0.94	0.10	0.00	0.00	3.35	0.97	0.81	1.93
Na	0.00	0.00	0.00	0.01	0.12	0.06	0.00	0.02	0.00	0.68	0.05	0.00	0.48
K	0.00	0.00	0.00	0.00	0.00	0.00	0.00	0.95	0.00	0.05	0.00	0.00	0.43
Sum	8.00	8.00	4.00	4.00	5.02	5.01	8.00	7.76	1.99	16.00	5.02	8.00	15.85
	$X_{Mg} = 0.14$ $X_{Fe} = 0.59$ $X_{Ca} = 0.23$	$X_{Mg} = 0.14$ $X_{Fe} = 0.67$ $X_{Ca} = 0.15$	$X_{Mg} = 0.49$ $X_{Fe} = 0.49$ $X_{Ca} = 0.02$	$X_{Mg} = 0.35$ $X_{Fe} = 0.17$ $X_{Ca} = 0.48$	$X_{Ca} = 0.88$ $X_{Na} = 0.12$	$X_{Ca} = 0.94$ $X_{Na} = 0.06$	$X_{Mg} = 0.19$ $X_{Fe} = 0.75$ $X_{Ca} = 0.03$	$X_{Mg} = 0.56$ $X_{Fe} = 0.44$		EqAn = 75	$X_{Ca} = 0.95$ $X_{Na} = 0.05$	$X_{Mg} = 0.03$ $X_{Fe} = 0.66$ $X_{Ca} = 0.27$	$X_{Mg} = 0.24$ $X_{Fe} = 0.76$

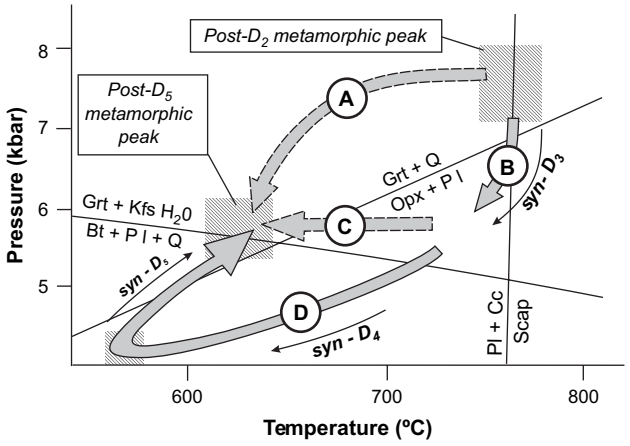

Fig. 10. Pressure-temperature diagram showing the possible retrograde trajectories followed by the Angul granulites following the post-D_2 metamorphic peak. Path A depicts single stage cooling and decompression to the post-D_5 metamorphic peak. Alternatively, path B implies initial (syn-D_3) decompression leading to garnet breakdown, followed either by isobaric cooling (path C), or cooling and decompression followed by renewed loading (path D). Path D explains renewed garnet formation on orthopyroxene-plagioclase symplectites in mafic granulites, and garnet formation on biotite in granitic melts; this is preferred by the present study.

following D_5 was characterized by comparatively lower temperatures and pressures (630 °C at ~5.5 kbar).

6. Discussion

6.1. The P-T path and radiometric ages – the case for reworking

In terms of the P-T trajectory, the change from M1 to M2 metamorphic conditions may be accomplished through a series of alternative paths (Fig. 10) – single stage cooling and decompression (path A); initial decompression followed by isobaric cooling (path B followed by C), or initial decompression and cooling, followed by renewed heating and loading (path B followed by D). The first two alternatives represent retrograde trajectories associated with a single orogenic event, while the third necessarily involves reworking of the crust during a separate tectonic cycle. Pressure-temperature calculations suggest that following the early granulite facies peak (M1) the region experienced decompression and cooling, and was uplifted into middle or even upper crustal domains. While D_5 structures indicate thrusting, the metamorphic evidence indicates that M2 was associated with increasing pressure and temperature, suggesting loading and heating of the terrane. This is more consistent with initial decompression and cooling followed by loading and heating (paths B and D), implying that the crust was definitely reworked in a separate orogenic event.

The timing of M1 metamorphism can be constrained from available radiometric age data from the Angul Domain. Monazites in garnet-sillimanite gneisses preserve an age of ca. 960 Ma; concordant sphene samples indicate ages ca. 930 Ma (Mezger and Cosca, 1999). Since monazites and sphenes have high closure temperatures with respect to the U-Pb system (e.g. Parrish, 1990; Mezger et al., 1991; Scott and St-Onge, 1995; Smith and Giletti, 1997), these ages correspond to the early granulite facies conditions that prevailed through, and outlasted the D_1 and D_2 deformation events. In the context of the present study, this age must correspond to M1 metamorphism in post-D_2 assemblages (750 °C). It is possible that peak temperatures during M1 may have been considerably higher and was initially followed by a period of slow isobaric cooling, as reported elsewhere in the Eastern Ghats Province (Dasgupta et al., 1991; Dasgupta and Sengupta, 1995).

The timing of M2 metamorphism, with peak temperatures of ca. 630 °C, is more difficult to constrain. Muscovite books in E-W trending, syn-D_4 pegmatites yield a Rb-Sr mineral age of 854 ± 6 Ma (Halden et al., 1982). Near identical ^{40}Ar-^{39}Ar cooling ages (845 ± 4 Ma) for amphibole have been obtained from the same area (Lisker and Fachmann, 2001). Since M2 metamorphism is correlated with D_5 deformation, it must correspond with later ages. In the Chilka Lake area of the northern EGB, post-Grenvillian transpressive deformation is estimated to have occurred at 662 ± 10 Ma (Dobmeier and Simmat, 2002). Scattered $^{40}Ar/^{39}Ar$ hornblende ages ranging from 650–570 Ma have also been reported from other parts of the EGB (Mezger and Cosca, 1999). Based on these arguments, M2 metamorphism may have occurred in the mid-Neoproterozoic (ca. 700–650 Ma). However, Mezger and Cosca (1999) attributed the scatter to incomplete resetting of Late Mesoproterozoic ages during a more distinct thermal overprint in Pan-African (Late Neoproterozoic-Cambrian) time. Pan-African $^{40}Ar/^{39}Ar$ cooling ages have also been specifically reported from the Rengali Province in the north, and the northern part of the EGP by Crowe et al. (2001) and Lisker and Fachmann (2001), but are commonly restricted to specific shear zones and associated with greenschist facies metamorphism (Crowe et al., 2003). Since M2 in this study is characterized by amphibolite facies conditions, the Late Neoproterozoic-Cambrian ages (550–500 Ma) are suggested to be correlatable with a later reactivation event along the EGP-Rengali Province boundary.

6.2. Tectonic evolution of the northern margin of the Eastern Ghats Province

After experiencing Late Mesoproterozoic-early Neoproterozoic granulite facies metamorphism with other parts of the Eastern Ghats Province, the Angul Domain underwent cooling and uplift (~850 Ma), followed by renewed tectonism during the mid-Neoproterozoic. This later tectonic event assumes importance in the context of the spatial proximity of the Angul Domain to the northern margin of the EGP. The structural study suggests that the Angul area was overthrust from the north; the metamorphic evidence concurrently confirms loading. Structures associated with this later tectonic imprint (i.e. D_5) on the Angul Domain can be correlated with those in the Rengali Province to the north (see Fig. 2), which is identified as a distinct lithotectonic block bound by the EGP and the Singhbhum cratonic nucleus (Mahalik, 1994; Nash et al.,

1996; Crowe et al., 2003). The Rengali Province comprises older granulite facies gneisses enclosed within amphibolite facies gneisses and supracrustals, and is separated from the EGP by a WNW-ESE trending discontinuity called the Kerajang Fault Zone (Nash et al., 1996; Crowe et al., 2003). North of this discontinuity, the Rengali Province is characterized by an amphibolite facies, WNW-ESE striking, north-dipping foliation related to southward directed thrusting. On the basis of similar hornblende $^{40}Ar/^{39}Ar$ cooling ages from the two terranes, Crowe et al. (2001, 2003) suggested that granulites of the EGP were juxtaposed during uplift against amphibolite facies rocks of the Rengali Province at ca. 700 Ma.

The results of this study indicate that the S_5 fabric in the Angul area can be correlated with the WNW trending, amphibolite facies S_{1-2} fabric in the Rengali Province. The latter is also associated with thrusting (Crowe et al., 2003). However, the metamorphic data suggests that M2 amphibolite facies metamorphism in Angul was associated with loading. Consequently, juxtaposition of the Rengali Province with the EGP occurred during thrusting associated with the later tectonic event, and not during uplift following initial granulite metamorphism as indicated by Crowe et al. (2003). Since the Angul Domain experienced loading prior to the M2 peak, the EGP is inferred to have been uplifted to shallower levels following D_4, and underwent renewed burial during the ca. 700 Ma reworking.

Palaeomagnetic studies (e.g., Torsvik et al., 2001a,b) indicate that the Indian craton was isolated through much of the Proterozoic (Powell and Pisarevsky, 2002; Pisarevsky et al., 2003; Collins and Pisarevsky, 2005). On the other hand, the EGB and the Rayner Complex of East Antarctica share petrological, structural and geochronological similarities that suggest contiguity in Late Mesoproterozoic to Neoproterozoic times (Dalziel, 1991; Hoffman, 1991; Chetty, 1995; Mezger and Cosca, 1999). The contact of the EGB with the Indian craton (Aftalion et al., 2000; Bhadra et al., 2004; Upadhyay et al., 2006; Dobmeier et al., 2006), and that of the Rayner Complex with the rest of Antarctica (Boger et al., 2001; Fitzsimons, 2003) are suggested to be of Late Neoproterozoic-Cambrian age, implying that this unit formed an exotic block through the Neoproterozoic (Dobmeier et al., 2006). Alternatively, the EGB-Rayner Complex combine may have been accreted (as an arc or microcontinent) to the Indian cratonic margin within the Neoproterozoic, but the bounding shear zones were reactivated during Late Neoproterozoic-Cambrian during collision with the rest of Antarctica along the Ruker Terrane-Prydz Bay region in Antarctica. Either way, the ca. 700 Ma reworking along the northern margin of the EGB must be considered a result of intracratonic deformation.

6.3. The signature of mid-crustal reworking

The results of this study demonstrate the extent to which mid-crustal reworking can camouflage the earlier tectonic history of a terrane. Reworking along the northern margin of the EGB led to the widespread overprinting and reorientation of earlier fabrics into the WNW-ESE orientations preserved in the lineament trends. Therefore, unlike some ancient orogens where a 'strike swing' can be related to the configuration of an ancient continental margin (e.g. Hutton and Alsop, 1996), the strike change in the northern part of the EGB can be attributed to a separate tectonic event. Since the WNW-ESE orientations characteristic of the northern margin of the belt are not observed further south within the granulite belt, the terrane boundaries of the EGB can be considered analogous to modern-day continental margins, that are inherently susceptible to reworking during later collisional orogenesis (Krabbendam, 2001). Reactivation of the Kerajang Fault Zone during the Late Neoproterozoic-Cambrian time (Crowe et al., 2003) confirms that the northern boundary of the Eastern Ghats Province, or EGB, remains susceptible to periodic adjustment during intracratonic deformation.

Almost all along the northern margin, evidence of the earlier tectonism has been completely obliterated, except in and around the town of Angul. The supracrustal assemblage preserved in this region possibly acted as a rigid unit during D_5 and partitioned strain around it, leading to diverging of the lineament trends and preservation of earlier tectonometamorphic imprints. Importantly, if this partitioning had not occurred, correlation of the WNW-ESE lineament trends with reworked structures, and identification of reworking itself would not have been possible.

Apart from the widespread overprinting, the deformation pattern in the 'low D_5 strain' Angul area also reflects how strain related to major shear zones is manifested away from the sites of shearing during mid-crustal deformation. In these regions, shear strain is accommodated along broader zones and is manifested as folds or warps on earlier fabrics. In the Angul area, almost all folds can be related to these bounding shears. Consequently, the widespread evidence for fold superposition in the gneisses does not necessarily reflect homogeneous strain accommodation within the terrane.

Importantly, amphibolite facies gneisses, that preserve metamorphic conditions corresponding to the mid-crust, are common constituents of all Precambrian terranes. These gneisses tend to preserve complex structural geometries characterized by the superposition of several phases of folding (e.g., Hopgood, 1980; Naha et al., 1990). Since fold superposition is observed on various scales, it appears that the mid-crust accommodates deformation homogeneously. However, the strain distribution during D_5 deformation in the Angul area, that operated under similar pressures and temperatures, indicates that folds on a mesoscopic-scale may possibly be related to major bounding shear zones. It is therefore possible that terranes characterized by superposed folding on a mesoscopic-scale, represent domains around which shear strain was partitioned during crustal-scale deformation. This, in turn, implies that within the crust, strain partitioning can occur even at depths of around 16 km and temperatures in excess of 600 °C.

Acknowledgements

SG and MKP gratefully acknowledge the financial support of the Department of Science and Technology, Government of India (Project No. ESS/16/199/2003). MS is grateful to the

Council of Science and Industrial Research for scholarship during the period of study. SG particularly acknowledges the contribution of Padmanava Debnath, Manasij Santra, Kathakali Bhattacharya, G.S. Rajesh, Debapriya Paul and Paromita Saha for assistance in the field at various stages of the study. Discussions with M.A. Mamtani were extremely beneficial. The manuscript has greatly improved from the suggestions of Alan Collins and Christoph Dobmeier, and Tom Blenkinsop's editorial advice.

References

Aftalion, M., Bowes, D.R., Dash, B., Dempster, T.J., 1988. Late Proterozoic charnockites in Orissa, India: A U-Pb and Rb-Sr isotopic study. Journal of Geology 96, 663–675.

Aftalion, M., Bowes, D.R., Dash, B., Fallick, A.E., 2000. Late Pan-African thermal history in the Eastern Ghats terrane, India, from U-Pb and K-Ar isotopic study of the Mid-Proterozoic Khariar alkali syenite, Orissa. Geological Survey of India Special Publications 57, 26–33.

Bhadra, S., Gupta, S., Banerjee, M., 2004. Structural evolution across the Eastern Ghats Mobile Belt – Bastar craton boundary, India: hot over cold thrusting in an ancient collision zone. Journal of Structural Geology 26, 233–245.

Bhattacharya, B., De, A., 1969. The sequence of deformation, metamorphism and igneous intrusion in the area around Angul (Orissa). Journal of the Geological Society of India 5, 159–171.

Boger, S.D., Wilson, C.J.L., Fanning, C.M., 2001. Early Palaeozoic tectonism within the East Antarctic craton: the final suture between east and west Gondwana? Geology 29, 463–466.

Bohlen, S.R., Wall, V.J., Boettcher, A.L., 1983. Experimental investigations and geological applications of equilibria in the system FeO-TiO_2-Al_2O_3-SiO_2-H_2O. American Mineralogist 68, 1049–1058.

Chetty, T.R.K., 1995. A correlation of Proterozoic shear zones between Eastern Ghats, India and Enderby Land, East Antarctica, based on LANDSAT imagery. Memoir of the Geological Society of India 34, 205–220.

Chetty, T.R.K., Murthy, D.S.N., 1998. Regional tectonic framework of the Eastern Ghats Mobile Belt: a new interpretation. Geological Survey of India. Special Publication 44, 39–50.

Collins, A.S., Pisarevsky, S.A., 2005. Amalgamating eastern Gondwana: the evolution of the Circum-Indian orogens. Earth Science Reviews 71 (3–4), 229–270.

Crowe, W.A., Cosca, M.A., Harris, L.B., 2001. $^{40}Ar/^{39}Ar$ geochronology and Neoproterozoic tectonics along the northern margin of the Eastern Ghats Belt in north Orissa, India. Precambrian Research 108, 237–266.

Crowe, W.A., Nash, C.R., Harris, L.B., Leeming, P.M., Rankin, L.R., 2003. The geology of the Rengali Province: implications for the tectonic development of northern Orissa, India. Journal of Asian Earth Sciences 21, 697–710.

Dalziel, I.W.D., 1991. Pacific margins of Laurentia and East Antarctica-Australia as a conjugate rift pair: evidence and implications for an Eocambrian supercontinent. Geology 19, 598–601.

Dasgupta, S., Sengupta, P., 1995. Ultrametamorphism in Precambrian granulite terrains – evidence from Mg-Al granulites and calc-granulites of the Eastern Ghats, India. Geological Journal 30, 307–318.

Dasgupta, S., Sengupta, P., Fukuoka, M., Bhattacharya, P.K., 1991. Mafic granulites from the Eastern Ghats, India: further evidence for extremely high crustal metamorphism. Journal of Geology 99, 124–133.

Dobmeier, C., Raith, M., 2003. Crustal architecture and evolution of the Eastern Ghats Belt and adjacent regions of India. In: Yoshida, M., Windley, B.F., Dasgupta, S. (Eds.), Proterozoic East Gondwana: Supercontinent Assembly and Breakup. Geological Society, London, Special Publications, vol. 206, pp. 145–168.

Dobmeier, C., Simmat, R., 2002. Post-Grenvillian transpression in the Chilka Lake area, Eastern Ghats Belt – implications for the geological evolution of peninsular India. Precambrian Research 113, 243–268.

Dobmeier, C., Lütke, S., Hammerschmidt, K., Mezger, K., 2006. Emplacement and deformation of the Vinukonda meta-granite (Eastern Ghats, India) – implications for the geological evolution of peninsular India and for Rodinia reconstructions. Precambrian Research 146, 165–178.

Ernst, W.G., Liu, J., 1998. Experimental phase-equilibrium study of Al- and Ti-contents of calcic amphibole in MORB – a semiquantitative thermobarometer. American Mineralogist 83, 952–969.

Ferry, J.M., Spear, F.S., 1978. Experimental calibration of the partitioning of Fe and Mg between biotite and garnet. Contributions to Mineralogy and Petrology 66, 113–117.

Fitzsimons, I.C.W., 2003. Proterozoic basement provinces of southern and southwestern Australia, and their correlation with Antarctica. In: Yoshida, M., Windley, B.F., Dasgupta, S. (Eds.), Proterozoic East Gondwana: Supercontinent Assembly and Breakup. Geological Society, London, Special Publications, vol. 206, pp. 93–130.

Graham, C.M., Powell, R., 1984. A garnet-hornblende thermometer: calibration, testing, and application to the Pelona schist, Southern California. Journal of Metamorphic Geology 2, 13–21.

Gupta, S., 2004. The Eastern Ghats Belt, India – a new look at an old orogen. Geological Survey of India. Special Publication 84, 75–100.

Gupta, S., Bhattacharya, A., Raith, M., Nanda, J.K., 2000. Pressure-temperature-deformational history across a vestigial craton-mobile belt boundary: the western margin of the Eastern Ghats Belt at Deobhog, India. Journal of Metamorphic Geology 18, 683–697.

Gupta, S., Panigrahi, M.K., Sarkar, M., 2005. The late stage evolution of the Angul migmatitic terrain, Eastern Ghats Belt, Orissa: constraints from integrated structural and fluid inclusion studies. Indian Journal of Geology 75, 147–166.

Halden, N.M., Bowes, D.R., Dash, B., 1982. Structural evolution of migmatites in granulite facies terrane: the Precambrian crystalline complex of Angul, Orissa, India. Transactions of the Royal Society of Edinburgh Earth Sciences 73, 109–118.

Harley, S.L., 1984. An experimental study of the partitioning of Fe and Mg between garnet and orthopyroxene. Contributions to Mineralogy and Petrology 86, 359–373.

Hoffman, P.F., 1991. Did the breakout of Laurentia turn Gondwanaland inside-out? Science 252, 1409–1412.

Holdsworth, R.E., Hand, M., Miller, J.A., Buick, I.S., 2001. Continental reactivation and reworking: an introduction. In: Miller, J.A., Holdsworth, R.E., Buick, I.S., Hand, M. (Eds.), Continental Reactivation and Reworking. Geological Society, London, Special Publications, vol. 184, pp. 1–12.

Holland, T.J.B., Powell, R., 1998. An internally consistent thermodynamic dataset for phases of petrological interest. Journal of Metamorphic Geology 16, 309–343.

Hopgood, A.M., 1980. Polyphase fold analysis of gneisses and migmatites. Transactions of the Royal Society of Edinburgh: Earth Sciences 71, 55–68.

Hopgood, A.M., 1999. Determination of Structural Successions in Migmatites and Gneisses. Kluwer Academic Publishers, Dordrecht.

Hutton, D.H.W., Alsop, G.I., 1996. The Caledonian strike-swing and associated lineaments in NW Ireland and adjacent areas: sedimentation, deformation and igneous intrusion patterns. Journal of the Geological Society of London 153, 345–360.

Krabbendam, M., 2001. When the Wilson Cycle breaks down: how orogens can produce strong lithosphere and inhibit future reworking. In: Miller, J.A., Holdsworth, R.E., Buick, I.S., Hand, M. (Eds.), Continental Reactivation and Reworking. Geological Society, London, Special Publications, vol. 184, pp. 57–75.

Lisker, S., Fachmann, S., 2001. The Phanerozoic history of Mahanadi region, India. Journal of Geophysical Research, B: Solid Earth 106, 22027–22050.

Mahalik, N.K., 1994. Geology of the contact between the Eastern Ghats Belt and the North Orissa Craton, India. Journal of Geological Society of India 44, 41–51.

Mahalik, N.K., 1996. Lithology and tectonothermal history of the Precambrian rocks of Orissa along the eastern coast of India. Journal of Southeast Asian Earth Sciences 14, 209–219.

Mezger, K., Cosca, M.A., 1999. The thermal history of the Eastern Ghats Belt (India) as revealed by U-Pb and ^{40}Ar-^{39}Ar dating of metamorphic and magmatic minerals: implications for the SWEAT correlation. Precambrian Research 94, 251–271.

Mezger, K., Rawnsley, C.M., Bohlen, S.R., Hanson, G.N., 1991. U-Pb garnet, sphene-monazite and rutile ages: implications for the duration of high grade metamorphism and cooling histories, Adirondack Mts., New York. Journal of Geology 99, 415–428.

Naha, K., Srinivasan, R., Jayaram, S., 1990. Structural evolution of the Peninsular Gneiss – an early Precambrian migmatitic complex from South India. Geologische Rundschau 79, 99–109.

Naqvi, S.M., Rogers, J.J.W., 1987. Precambrian Geology of India. Oxford University Press, New York.

Nash, C.R., Rankin, L.R., Leeming, P.M., Harris, L.B., 1996. Delineation of lithostructural domains in northern Orissa (India) from Landsat Thematic Mapper imagery. Tectonophysics 260, 245–257.

Newton, R.C., Perkins, D.I., 1982. Thermodynamic calibration of geobarometers based on the assemblages garnet-plagioclase-orthopyroxene (clinopyroxene)-quartz. American Mineralogist 67, 203–222.

Parrish, R.R., 1990. U-Pb dating of monazite and its application to geological problems. Canadian Journal of Earth Sciences 27, 1435–1450.

Pisarevsky, S.A., Wingate, M.T.D., Powell, C.M., Johnson, S., Evans, D.A.D., 2003. Models of Rodinia assembly and fragmentation. In: Yoshida, M., Windley, B.F., Dasgupta, S. (Eds.), Proterozoic East Gondwana: Supercontinent Assembly and Breakup. Geological Society, London, Special Publications, vol. 206, pp. 35–55.

Powell, C.M.A., Pisarevsky, S., 2002. Late Neoproterozoic assembly of East Gondwana. Geology 30, 3–6.

Ramakrishnan, M., Nanda, J.K., Augustine, P.F., 1998. Geological evolution of the Proterozoic Eastern Ghats Mobile Belt. Geological Survey of India. Special Publication 44, 1–21.

Ramsay, J.G., 1967. Folding and Fracturing of Rocks. McGraw-Hill, New York.

Rickers, K., Mezger, K., Raith, M.M., 2001. Evolution of the continental crust in the Proterozoic Eastern Ghats Belt, India and new constraints for Rodinia reconstruction: implications from Sm-Nd, Rb-Sr and Pb-Pb isotopes. Precambrian Research 112, 183–210.

Ring, U., 1994. The influence of pre-existing structure on the evolution of the Cenozoic Malawi Rift (East African Rift System). Tectonics 13 (2), 313–326.

Roering, C., van Reenen, D.D., De Beer, J.H., Smit, C.A., Barton Jr., J.M., De Wit, M.J., Stettler, E.J., Van Schalkwyk, J.F., Stevens, G., Pretorious, S., 1992. Tectonic model for the evolution of the Limpopo Belt. Precambrian Research 55, 539–552.

Scott, D.J., St-Onge, M.R., 1995. Constraints on Pb closure temperature in titanite based on rocks from the Ungava orogen, Canada: implications for U-Pb geochronology and *P-T-t* path determinations. Geology 23, 1123–1126.

Smith, H.A., Giletti, B.J., 1997. Pb diffusion in monazite. Geochimica et Cosmochimica Acta 61, 1047–1055.

Torsvik, T.H., Ashwal, L.D., Tucker, R.D., Eide, E.A., 2001a. Neoproterozoic geochronology and palaeogeography of the Seychelles microcontinent: the India link. Precambrian Research 110, 47–59.

Torsvik, T.H., Carter, L.M., Ashwal, L.D., Bhushan, S.K., Pandit, M.K., Jamtveit, B., 2001b. Rodinia refined or obscured: paleomagnetism of the Malani igneous suite (NW India). Precambrian Research 108, 319–333.

Upadhyay, D., Raith, M., Mezger, E.K., Bhattacharya, A., Kinny, E.P.D., 2006. Mesoproterozoic rifting and Pan-African continental collision in SE India: evidence from the Khariar alkaline complex. Contributions to Mineralogy and Petrology 151 (4), 434–456.

Vauchez, A., Barruol, G., Tommasi, A., 1997. Why do continents break up parallel to ancient orogenic belts? Terra Nova 9, 62–66.

Wheeler, J., 1987. The determination of true shear senses from the deflection of passive markers in shear zones. Journal of the Geological Society of London 144, 73–77.